引用格式：ZHANG Hongwei, QU Rui, CHEN Weining, et al. Design of Optical-mechanical System of Catadioptric Aerial Mapping Camera Based on Secondary Mirror Image Motion Compensation[J]. Acta Photonica Sinica, 2024, 53(2):0222001
张洪伟,曲锐,陈卫宁,等.基于次镜像移补偿的折反式航测相机光机系统设计[J].光子学报,2024,53(2):0222001

基于次镜像移补偿的折反式航测相机光机系统设计

张洪伟,曲锐,陈卫宁,杨洪涛
(中国科学院西安光学精密机械研究所 飞行器光学成像监视与测量技术研究室,西安 710119)

摘　要:针对航测相机对地摆扫成像过程中的动态像移问题,采用两镜望远系统的矢量像差理论,将次镜作为像移补偿元件,通过次镜多维运动实现航测相机的综合像移补偿。次镜在对像移进行补偿的过程中会发生偏心和倾斜,导致次镜离轴,影响成像质量,因此,建立了失调折反光学系统成像模型,研究次镜像差场偏移矢量与次镜失调量之间的关系,并分析次镜多维运动对成像质量的影响。为验证次镜多维运动的像移补偿能力,搭建实验平台对该航测相机进行了实验室内以及外场成像试验。结果表明,采用该像移补偿技术的航测相机动态分辨率可达 74 lp/mm,且像移补偿精度优于 0.5 个像素,达到设计预期。

关键词:航测相机;像移补偿技术;光机系统;次镜失调;矢量像差理论
中图分类号:V241;TP73　　**文献标识码**:A　　**doi**:10.3788/gzxb20245302.0222001

0　引言

航空测绘是民用测绘的重要技术手段,可在短时间内快速获取目标区域大范围、高精度的比例尺成图,并对地图上的目标平面坐标信息和高程信息进行精确获取,这些信息的获取对数字城市建设、国土资源普查等具有重要的支撑作用[1-2]。

随着航测相机应用要求的逐渐提高,对航测相机宽幅成像及高精度大比例尺成图的需求日益迫切。目前国内外航空面阵测绘相机的技术途径有两种,分别为固定式多镜头拼接测量成像和摆扫式测量成像。与固定式多镜头拼接测绘相机相比,摆扫式测绘相机可采用较少的镜头数量实现较大成像幅宽,同时还可以通过调整稳定平台角度实现大倾斜远距离测量成像。由于载机姿态变化及自身振动会导致曝光成像时间内地物目标与探测器之间产生相对运动,带来前向像移、扫描像移以及振动像移,影响成像质量。为满足长焦距测绘相机的稳像精度,通常采用具有二级稳像功能的两轴四框架稳定平台,但其有效载荷占比低,不满足小型化、轻量化要求。

本文航测相机采用折反式光学系统中的次镜与二级稳像功能相结合的设计理念,通过次镜快速运动实现高精度的像移补偿以及指向测量。经实物样机试验验证,所设计的航测相机具有高精度的像移补偿功能,并且能够满足小型化、轻量化、高精度大比例尺成图的要求。

1　次镜稳像的矢量像差理论

折反式光学系统一般由两反望远镜系统和校正镜组构成,在本文光学系统中两反望远镜系统采用R-C结构形式,校正镜组采用透镜和双胶合镜组合的结构形式。次镜在像移补偿过程中会发生偏心和倾斜,导

基金项目:中国科学院青年创新促进会项目(No. 2023422)
第一作者:张洪伟, zhanghongwei@opt.ac.cn
通讯作者:杨洪涛, yanght@opt.ac.cn
收稿日期:2023-07-18;**录用日期**:2023-09-26

致次镜离轴，次镜离轴后R-C系统失去原有的系统对称性，传统的像差模型不再适用，需要引入矢量像差理论[3-6]。

1.1 次镜离轴对一阶参数的影响

为了更好地阐述次镜补偿像移的工作原理，需要建立失调光学系统模型，研究次镜像差场偏移矢量与次镜失调量之间的关系[7-10]。由次镜运动引起的光学系统像点位置的偏移量可通过光轴光线追迹到像平面获得，如图1所示。

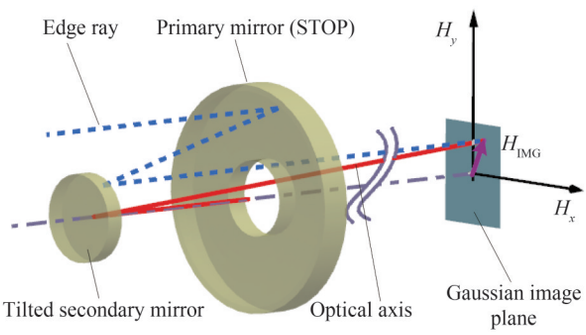

图1 次镜失调量与像差场偏移矢量关系

Fig. 1 The relationship between the amount of secondary mirror misalignment and the aberration field offset vector

根据离轴矢量像差理论，由次镜运动引起的光学系统像点位置的偏移量$\boldsymbol{H}_{\mathrm{IMG}}$可表示为

$$H_{\mathrm{IMG}}=\sqrt{H_{x\_\mathrm{IMG}}{}^{2}+H_{y\_\mathrm{IMG}}{}^{2}} \tag{1}$$

式中，像点位置偏移量$\boldsymbol{H}_{\mathrm{IMG}}$在像平面$X$轴和$Y$轴的向量分量$\boldsymbol{H}_{x_\mathrm{IMG}}$、$\boldsymbol{H}_{y_\mathrm{IMG}}$可表示为

$$\begin{cases}\begin{bmatrix}H_{x\_\mathrm{IMG}}\\H_{y\_\mathrm{IMG}}\end{bmatrix}=\dfrac{\beta L(1-m)}{(f'_{\mathrm{SYS}})\gamma\bar{y}_{\mathrm{IMG}}}\begin{bmatrix}E_{\mathrm{SM}\_x}-\dfrac{2\gamma(f'_{\mathrm{SYS}})}{1-m}\varphi_{\mathrm{SM}\_y}\\E_{\mathrm{SM}\_y}+\dfrac{2\gamma(f'_{\mathrm{SYS}})}{1-m}\varphi_{\mathrm{SM}\_x}\end{bmatrix}\\L=\gamma f'_{\mathrm{SYS}}\\m\equiv-\dfrac{f'_{\mathrm{SYS}}}{f'_{\mathrm{PM}}}\end{cases} \tag{2}$$

式中，β为校正镜组放大倍率，γ为遮拦比，L为次镜非球面顶点到高斯像面的距离，f'_{SYS}为望远系统焦距，f'_{PM}为主镜焦距，$\bar{y}_{\mathrm{IMG}}$为图像坐标系主光轴高，$E_{\mathrm{SM}_x}/E_{\mathrm{SM}_y}$为次镜偏心量，$\varphi_{\mathrm{SM}_x}/\varphi_{\mathrm{SM}_y}$为次镜倾斜量。

为方便计算，将式(2)进一步推导可得

$$\begin{bmatrix}H_{x\_\mathrm{IMG}}\\H_{y\_\mathrm{IMG}}\end{bmatrix}=\frac{\beta}{\bar{y}_{\mathrm{IMG}}}\begin{bmatrix}(1-m)E_{\mathrm{SM}\_x}-(2L)\varphi_{\mathrm{SM}\_y}\\(1-m)E_{\mathrm{SM}\_y}+(2L)\varphi_{\mathrm{SM}\_x}\end{bmatrix} \tag{3}$$

1.2 次镜离轴引入的三级像差

由于三级球差与视场大小无关，而次镜离轴只对像差的视场相关性有影响，故次镜运动在不改变R-C系统主次镜轴向间隔的情况下，三级球差不受次镜离轴的影像。次镜离轴对光学系统成像的影像主要体现在三级彗差和三级像散上，三级彗差与视场大小成线性关系，并且只有一个彗差节点；三级像散与视场大小成平方关系，并且有两个像散节点。

根据矢量像差理论，在失调R-C系统中，三级彗差可表示为

$$W_{\mathrm{COMA3}}=\begin{bmatrix}-A_{131,x}\\-A_{131,y}\end{bmatrix}\cdot[\boldsymbol{\rho}](\boldsymbol{\rho}\cdot\boldsymbol{\rho}) \tag{4}$$

$$\begin{bmatrix}A_{131,x}\\A_{131,y}\end{bmatrix}=\begin{bmatrix}\sigma_{\mathrm{SM},x}^{(sph)}&\sigma_{\mathrm{SM},x}^{(asph)}\\\sigma_{\mathrm{SM},y}^{(sph)}&\sigma_{\mathrm{SM},y}^{(asph)}\end{bmatrix}\begin{bmatrix}W_{131,\mathrm{SM}}^{sph}\\W_{131,\mathrm{SM}}^{asph}\end{bmatrix} \tag{5}$$

式中，W_{131}为三级彗差系数，$\boldsymbol{\sigma}_{\mathrm{SM}}^{(sph)}$为归一化球面像差偏心矢量，$\boldsymbol{\sigma}_{\mathrm{SM}}^{(asph)}$为归一化非球面像差偏心矢量。

根据式(5)可知，当$A_{131}=0$时，次镜离轴对三级彗差的影响可相互抵消，即系统光轴存在一个无彗差枢

纽点。当次镜绕这一枢纽点旋转时，次镜运动不会改变三级彗差场。次镜顶点到无彗差枢纽点的距离L_{SM}^{cfp}可表示为

$$L_{\mathrm{SM}}^{cfp}=\frac{2f'_{\mathrm{SYS}}\gamma(\gamma-1)W_{131,\mathrm{SM}}^{sph}}{[1-m-(m+1)\gamma]W_{131,\mathrm{SM}}^{asph}-(1-m)(\gamma-1)W_{131,\mathrm{SM}}^{sph}} \tag{6}$$

同样地，失调R-C系统的三级像散可表示为

$$W_{\mathrm{ATS3}}=\frac{1}{2}\left[W_{222}H^2-2HA_{222}+B_{222}^2\right](\boldsymbol{\rho}^2) \tag{7}$$

$$\begin{bmatrix}A_{222,x}\\A_{222,y}\\B_{222,x}^2\\B_{222,y}^2\end{bmatrix}=\begin{bmatrix}\boldsymbol{\sigma}_{\mathrm{SM},x}^{(sph)} & \boldsymbol{\sigma}_{\mathrm{SM},x}^{(asph)}\\ \boldsymbol{\sigma}_{\mathrm{SM},y}^{(sph)} & \boldsymbol{\sigma}_{\mathrm{SM},y}^{(asph)}\\ \boldsymbol{\sigma}_{\mathrm{SM},x}^{(sph)2}-\boldsymbol{\sigma}_{\mathrm{SM},y}^{(sph)2} & \boldsymbol{\sigma}_{\mathrm{SM},x}^{(asph)2}-\boldsymbol{\sigma}_{\mathrm{SM},y}^{(asph)2}\\ 2\boldsymbol{\sigma}_{\mathrm{SM},x}^{(sph)}\boldsymbol{\sigma}_{\mathrm{SM},y}^{(sph)} & 2\boldsymbol{\sigma}_{\mathrm{SM},x}^{(asph)}\boldsymbol{\sigma}_{\mathrm{SM},y}^{(asph)}\end{bmatrix}\begin{bmatrix}W_{222,\mathrm{SM}}^{sph}\\W_{222,\mathrm{SM}}^{asph}\end{bmatrix} \tag{8}$$

次镜离轴引入的三级像散呈“双节点”现象，像散节点在视场中的位置可表示为

$$H_{\mathrm{ATS3}}=\frac{A_{222}}{W_{222}}\pm i\sqrt{\frac{B_{222}^2}{W_{222}}-\left(\frac{A_{222}}{W_{222}}\right)^2} \tag{9}$$

1.3 次镜像移补偿工作原理

次镜的像移补偿是通过次镜的快速偏转运动，实现航测相机在成像过程中高精度稳定成像，如图2。

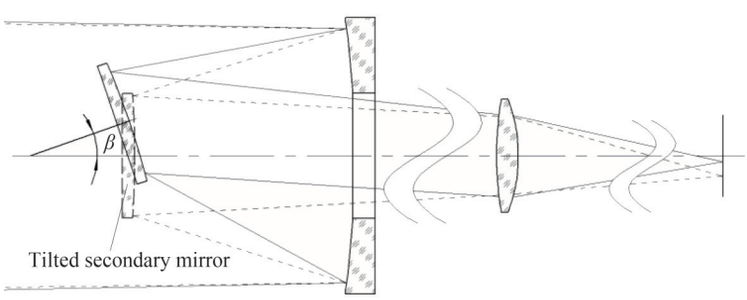

图2 折反式光学系统次镜像移补偿原理

Fig. 2 Image motion compensation principle of the catadioptric mapping camera

根据上述分析，将次镜旋转中心定为无彗差枢纽点，根据如图3所示的几何关系，当次镜倾斜量φ_{SM_x}/φ_{SM_y}较小时，次镜偏心量可以简化为

$$\begin{bmatrix}E_{\mathrm{SM}\_x}\\E_{\mathrm{SM}\_y}\end{bmatrix}=\begin{bmatrix}L_{\mathrm{SM}}^{cfp}\times\sin\left(\varphi_{\mathrm{SM}\_y}\times 180/\pi\right)\\ L_{\mathrm{SM}}^{cfp}\times\sin\left(\varphi_{\mathrm{SM}\_x}\times 180/\pi\right)\end{bmatrix}\approx\begin{bmatrix}L_{\mathrm{SM}}^{cfp}\times\varphi_{\mathrm{SM}\_y}\\ L_{\mathrm{SM}}^{cfp}\times\varphi_{\mathrm{SM}\_x}\end{bmatrix} \tag{10}$$

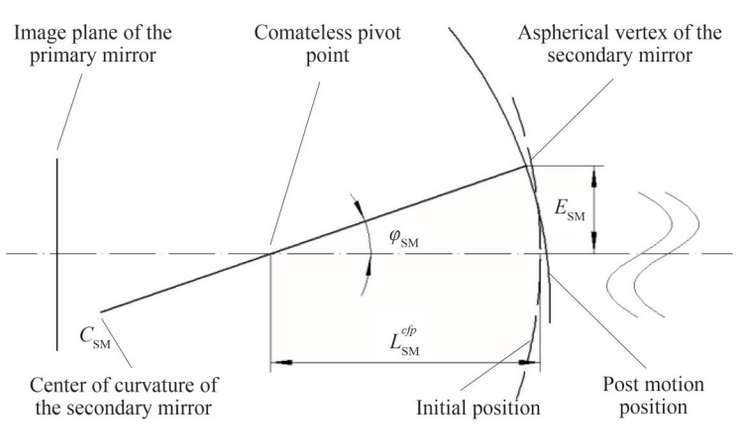

图3 次镜运动引入的偏心矢量

Fig. 3 Eccentricity vector introduced by the motion of the secondary mirror

将式(10)带入式(3)可得

$$\begin{bmatrix} H_{x\_\mathrm{IMG}} \\ H_{y\_\mathrm{IMG}} \end{bmatrix} = \frac{\beta}{\bar{y}_{\mathrm{IMG}}} \begin{bmatrix} \left((1-m)L_{\mathrm{SM}}^{cfp} - 2L\right)\varphi_{\mathrm{SM}\_y} \\ \left((1-m)L_{\mathrm{SM}}^{cfp} + 2L\right)\varphi_{\mathrm{SM}\_x} \end{bmatrix} \tag{11}$$

由式(11)可知,当次镜绕无彗差枢纽点旋转角较小时,像点位置偏移量H_{x_IMG}、H_{y_IMG}与次镜偏转角呈线性关系。因此,当像点位置偏移量H_{x_IMG}与相机曝光时刻的像移量H_{Motion}之间的关系满足式(12)时,便可实现对像移的完全补偿。

$$H_{\mathrm{IMG}} = -H_{\mathrm{Motion}} \tag{12}$$

2 次镜稳像的航测相机光机系统设计

2.1 系统参数及光机系统设计

航测相机光学系统的主要参数包括焦距、视场角、相对口径等。受衍射极限的限制,航测相机光学系统的最小分辨率往往取决于系统的相对口径。本文航测相机的成像靶面选用5 120×3 840面阵探测器,像元尺寸为6.4 μm。综合考虑航测相机的飞行参数、体积尺寸、质量、成图性能等因素,系统参数如表1。

表1 系统参数

Table 1 System parameters

Parameter		Value
Flight parameters	Flight speed	180~280 km/h
	Flight height	1~7.5 km
	Working temperature	−40 ℃~+60 ℃
Camera parameters	Spectrum	435~900 nm
	Effective focal length	450 mm
	Field of view	4.17°×3.13°
	F-number	4.2
	MTF	≥0.2 (80 lp/mm @ all FOV)

光学系统设计以折反结构形式为基础进行次镜离轴复杂化设计。光学系统中的两反望远镜系统采用R-C结构形式,在次镜与焦平面之间插入一组校正镜组,用于扩大系统视场;校正镜组包含一组双胶合镜,用于校正较宽谱段引入的色差[11-13];通过匹配光学材料与结构材料实现光学系统的无热化设计[14-16]。光学镜头采用分光棱镜将全色光分成R、G、B和近红外四个谱段,并进行分别成像,如图4。采用光谱校正技术和谱段配准技术,实现可见光全色/RGB和近红外成像要求,航测相机结构模型如图5。

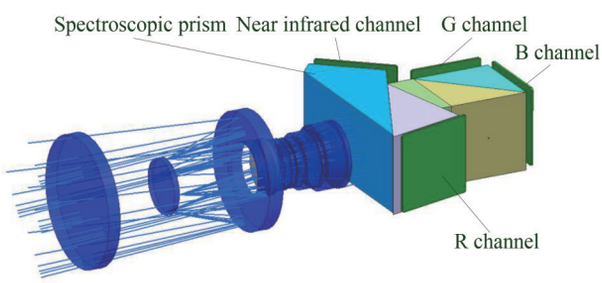

图4 航测相机光学系统及分光棱镜示意

Fig. 4 Schematic of aerial mapping camera optical system and spectroscopic prisms

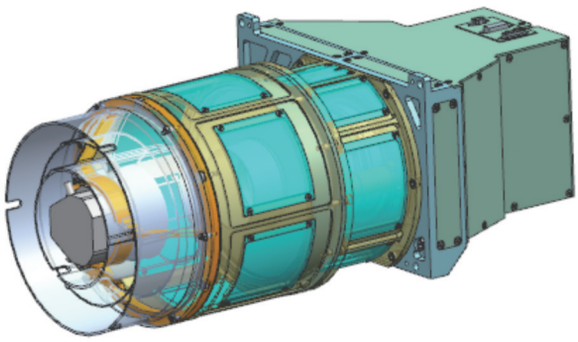

图5　光学成像相机结构模型

Fig. 5　Structure model of optical imaging camera

2.2　像质评价

航测相机光学系统全色谱段的空间采样Nyquist频率为80 lp/mm，在中心遮拦比（面积）为26.3%、次镜处于零位时，全视场调制传递函数优于0.32。另外，次镜的偏转会引入三阶像差，在次镜绕无彗差枢纽点偏转0.01°、0.03°、0.05°条件下，全视场传函如图6。从图中可以看出，次镜在不同偏转角度下的全视场调制传递函数均大于0.2，可以保证光学镜头优良的成像质量。

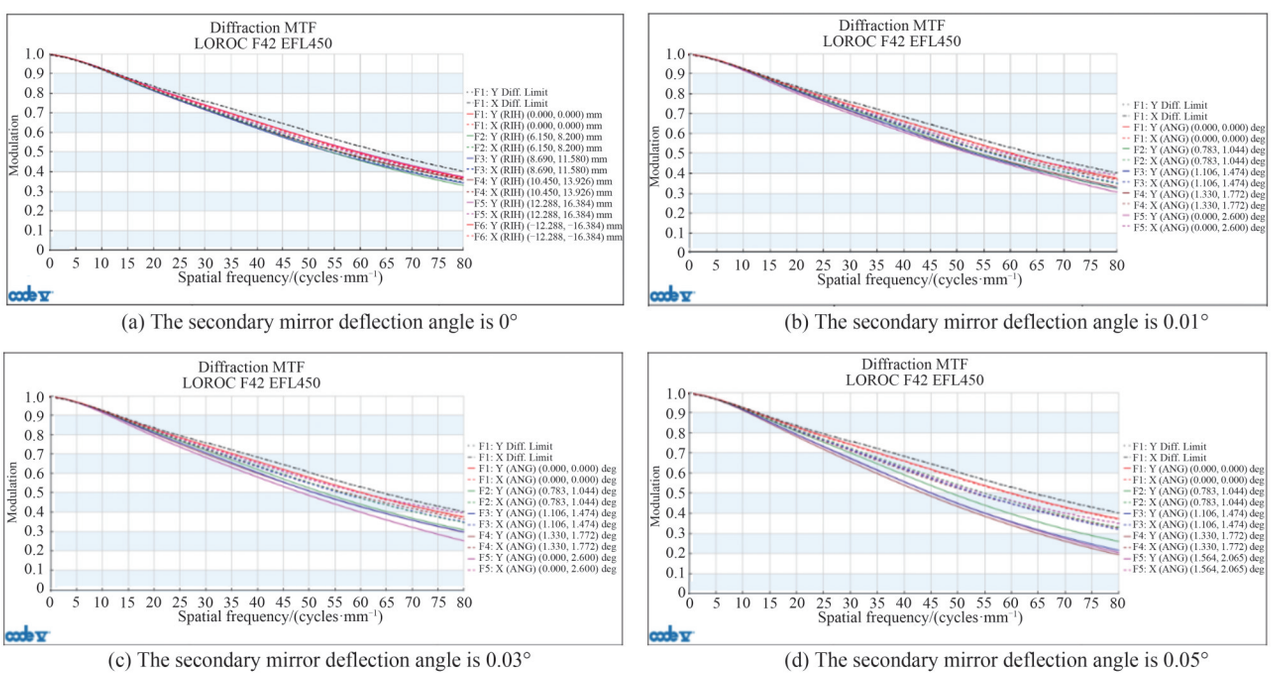

(a) The secondary mirror deflection angle is 0°

(b) The secondary mirror deflection angle is 0.01°

(c) The secondary mirror deflection angle is 0.03°

(d) The secondary mirror deflection angle is 0.05°

图6　次镜在不同偏转角度下的光学系统传函

Fig. 6　MTF of the optical system under different deflection angles of secondary mirror

3　试验与结果

3.1　实验室内成像试验

为验证次镜像移补偿机构的二维像移补偿能力，对其进行实验室内成像试验。成像试验用到的仪器设备主要为3 m平行光管，其主要过程是通过调节二维稳定平台的俯仰及横滚扫描速率精确模拟目标（4号鉴别率板、十字靶标）在不同速高比、不同扫描速率下的姿态速率，同时二维振镜驱动次镜运动，补偿目标移动带来的像移，如图7。实验中，二维稳定平台横滚扫描速度+60°/s，俯仰扫描速度为5°/s，经过试验测试可得：相机可分辨4号鉴别率板第11组条纹（11.1 lp/mm），证明相机动态分辨率可达74 lp/mm，达到设计预期；对十字靶标成像，十字靶标试验前、试验过程中靶标点移动量为0.5个像素，即二维像移补偿精度为0.5个像素。

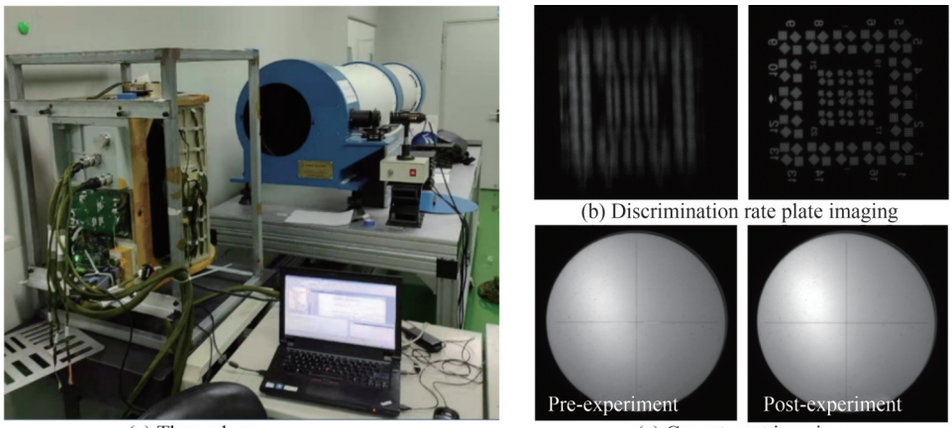

图7 实验室内二维像移补偿试验

Fig. 7 Two-dimensional image motion compensation test

3.2 外场飞行成像试验

外场飞行成像试验过程中，同步开展了综合像移补偿性能测试。图8为载机在飞行速度242 km/h、飞行高度3.17 km飞行工况下，分别开启和关闭综合像移补偿机构所采集到的图像。从图中可以明显看出，开启综合像移补偿功能后的航测相机采集到图像的像移得到有效补偿，达到预期要求。

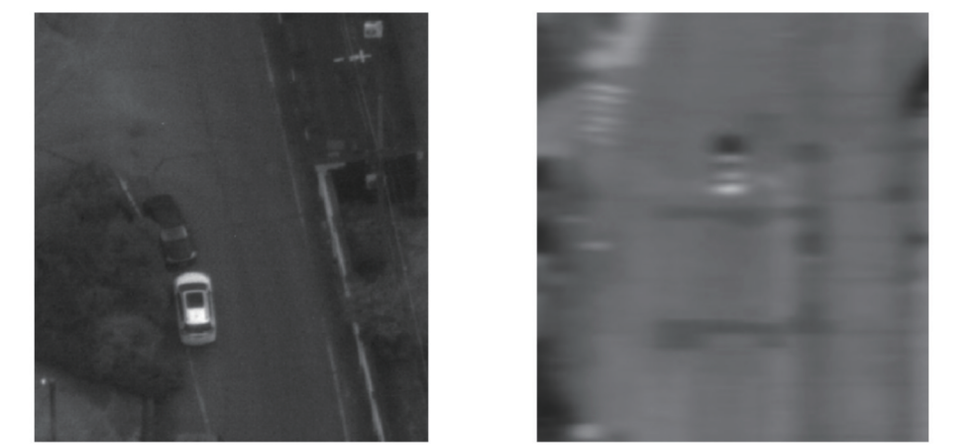

图8 综合像移补偿外场成像试验

Fig. 8 Comprehensive image motion compensation outfield imaging test

4 结论

本文建立了失调两镜望远系统的成像模型，将折反光学系统中的次镜作为像移补偿元件，通过次镜的偏转运动实现了航测相机工作过程中前向/扫描/振动像移的综合补偿。通过对基于次镜像移补偿的航测相机进行实验室内成像试验可知，采用次镜偏转运动进行像移补偿的航测相机的动态分辨率可达74 lp/mm，且该像移补偿方法的精度优于0.5个像素。经过飞行试验，基于次镜像移补偿的航测相机工作稳定可靠，并获得了高质量的图像。试验证明，该航测相机具有像移补偿精度高、结构紧凑、可靠性高等优点，可为航测相机朝轻小型、高精度大比例尺成图的方向发展奠定理论基础。

参考文献

[1] GUERRERO J, GUTIERREZ F, CARBONEL D, et al. 1∶5000 landslide map of the upper Gállego valley (central spanish pyrenees)[J]. Journal of Maps, 2012, 8(4): 484-491.

[2] YALCIN G, SELCUK O. 3D city modelling with oblique photogrammetry method[J]. Procedia Technology, 2015, 19: 424-431.

[3] CHE Chicheng, LI Yingcai, FAN Xuewu, et al. Research on computer-aided alignment based on vector aberration theory

[J]. Acta Photonica Sinica, 2008, 52(8): 1630-1634.
车驰骋,李英才,樊学武,等.基于矢量波像差理论的计算机辅助装调技术研究[J].光子学报,2008,52(8):1630-1634.
[4] LAIRD M C, DONALD W M. Infrared imaging using a tip-tilt secondary mirror[C]. SPIE , 1993,1920:353-363.
[5] XUEJI L, DONGMING Y, LAIYUN S, et al. Two-mirror aerial mapping camera design with a tilted-aplanatic secondary mirror for image motion compensation[J]. Optics Express, 2023,31(3):4108-4121.
[6] ZOU Gangyi, FAN Xuewu, PANG Zhihai, et al. Design of unobscured three-mirror optical system by applying vector wavefront aberration theory[J]. Infrared and Laser Engineering, 2014, 43(2): 569-573.
邹刚毅,樊学武,庞志海,等.矢量波像差理论在无遮拦三反光学系统设计中的应用[J].红外与激光工程,2014,43(2):569-573.
[7] KONG Xiaohui. Study on computer aided alignment for two mirror reflect optical system[D]. Xi′an:Xi′an Institute of Optics and Precision Mechanics Chinese Academy of Science, 2010.
孔小辉.两镜系统计算机辅助装调研究[D].西安:中国科学院研究生院(西安光学精密机械研究所), 2010.
[8] SCHMID T. Misalignment induced nodal aberration fields and their use in the alignment of astronomical telescopes [D]. Orlando:University of Central Florida, 2010.
[9] SCHMID T, THOMPSON K P, ROLLAND J P. Misalignment-induced nodal aberration fields in two-mirror astronomical telescopes[J]. Applied Optics, 2010,49(16):131-144.
[10] GU Zhiyuan. Misalignment corrections in reflective telescopes[D]. Changchun: Changchun Institute of Optics, Fine Mechanics and Physics, Chinese Academy of Science, 2016.
顾志远.反射式望远镜失调校正技术研究[D].长春:中国科学院研究生院(长春光学精密机械与物理研究所), 2016.
[11] GALAN M, STROJNIK M, WANG Y. Design method for compact, achromatic, high-performance, solid catadioptric system (SoCatS), from visible to IR[J]. Optics Express, 2019, 27(1):142-149.
[12] LAIKIN M. Lens design[M]. 4th ed. Boca Raton: CRC Press, 2018.
[13] LIM T Y, PARK S C. Design of a catadioptric system with corrected color aberration and flat petzval curvature using a graphically symmetric method[J]. Current Optics and Photonics , 2018, 2(4): 324-331.
[14] XIE N, CUI Q, SUN L, et al. Optical athermalization in the visible waveband using the 1+∑ method[J]. Applied Optics, 2019, 58(3): 635-641.
[15] ZHU J, HEN W. Analytical design of athermal ultra-compact concentric catadioptric imaging spectrometer[J]. Optics Express, 2019, 27(21): 31094-31109.
[16] ZHU Y, CHENG J, LIU Y. Multiple lenses athermalization and achromatization by the quantitative replacement method of combined glasses on athermal visible glass map[J]. Optics Express, 2021, 29(21): 34707-34722.

Design of Optical-mechanical System of Catadioptric Aerial Mapping Camera Based on Secondary Mirror Image Motion Compensation

ZHANG Hongwei, QU Rui, CHEN Weining, YANG Hongtao
(*Aircraft Optical Imaging and Monitoring and Measurement Technology Laboratory, Xi′an Institute of Optics and Precision Mechanics, Chinese Academy of Sciences, Xi′an* 710119, *China*)

Abstract: Aerial surveying and mapping is an important technical means of civil/military surveying and mapping, which can quickly obtain large-scale and high-precision scale mapping of the target area in a short period of time, and accurately obtain coordinate information of the target plane and elevation information on the map. The acquired information plays an important supporting role in digital city construction, land resources survey, military strategic planning, etc. With the development of aerial surveying and mapping technology, the requirements for aerial mapping cameras have been further improved. It is required that aerial mapping cameras can achieve wide width, high precision and large scale mapping. In order to meet the above requirements, the aerial mapping camera adopts scan imaging mode, but this imaging mechanism will introduce forward/scan image motion, which will affect the image quality. In order to satisfy the image stabilization accuracy of the aerial mapping camera, it is necessary to compensate the image motions. Therefore, a catadioptric aerial mapping camera based on secondary mirror image motion compensation is designed in this paper.

Aiming at the dynamic image motion problem of the aerial mapping camera in the process of ground swing imaging, the vector aberration theory for a two-mirror telescopic systems is adopted. The secondary

mirror is used as the image motion compensation element, and the comprehensive image motion compensation of the aerial mapping camera is realized through the secondary mirror multi-dimensional motion. However, in the process of compensating the image motion, the secondary mirror will be eccentric and inclined, which will cause the secondary mirror to be off-axis and affect the image quality. Therefore, a misalignment optical system model is established to study the relationship between the deviation vector of the secondary mirror field and the misalignment of the secondary mirror field, and the influence of the secondary mirror motion on the image quality is analyzed. Meanwhile, a design example of the optical-mechanical system of the catadioptric aerial mapping camera based on the secondary mirror image motion compensation is given. The effective focal length of the optical system is 450 mm, and the working spectrum is 435～900 nm. The field of view of the optical system is 4.17×3.13, and the F-number is 4.2. In the design process, the optical-mechanical system of aerial mapping camera adopts non-thermal design to adapt to the working environment of －40 ℃～60 ℃.

In order to verify the image motion compensation ability of multi-dimensional motion of the optical element, an experimental platform is built to conduct laboratory imaging tests and field imaging tests on the aerial mapping camera. The laboratory imaging test results show that the dynamic resolution of the aerial mapping camera using the image motion compensation technology can reach 74 lp/mm, and the image motion compensation accuracy is better than 0.5 pixels, which meets the design expectation. In addition, the field imaging test results show that compared with disable image motion compensation function, the aerial survey camera with enable image motion compensation function can acquire sharp edges, clear images, and image quality can meet the expected requirements. Therefore, the camera has the advantages of high accuracy of image motion compensation, compact volume and high reliability, which lays a theoretical foundation for the direction of light and small, high precision and large scale mapping.

Key words: Aerial mapping camera; Image motion compensation technology; Optical-mechanical system; Secondary mirror misalignment; Vector aberration theory

OCIS Codes: 220.1000; 120.3620; 120.4640; 220.3620

Foundation item: Youth Innovation Promotion Association of the Chinese Academy of Sciences (No. 2023422)